Microfluid Nanofluid (2015) 18:1255–1263
DOI 10.1007/s10404-014-1524-6

RESEARCH PAPER

Characterization of a high-resolution solid-state micropump that can be integrated into microfluidic systems

Aaron R. Smith · Andrey Saren · Jari Järvinen · Kari Ullakko

Received: 1 July 2014 / Accepted: 2 December 2014 / Published online: 8 January 2015

Abstract Ni–Mn–Ga is a magnetic shape memory (MSM) alloy that can strain up to 6 % when a magnetic field is applied to it. By applying a localized magnetic field to the MSM element, the strain can be precisely controlled and manipulated. By using Ni–Mn–Ga and a local magnetic field, an MSM micropump that is capable of controlling the flow within a microfluidic system has been developed. A computational fluid dynamics analysis illustrates the flow of the liquid at the outlet of the micropump and will be used to optimize future models of the pump. The performance of the MSM micropump, such as its flow rate and pumping pressure, is measured and presented in this study. Beyond its performance, there are also several advantages intrinsic to the MSM micropump. It is controlled by a magnetic field and is therefore contact-free. Depending upon the magnetic field, the MSM micropump can act as either a valve or a reversible pump. It is self-priming and capable of pumping gases as well as viscous liquids, and it has a simple design which consists primarily of the MSM alloy itself. Coupled with its scalability, it is clear that the MSM micropump is a strong candidate for an integratable flow control solution.

Keywords Magnetic shape memory · Ni–Mn–Ga · Micropump · Lab-on-a-chip · Microfluidic device

A. R. Smith · A. Saren · K. Ullakko (✉)
Lappeenranta University of Technology, LUT Chemtech, Laitaatsillantie 3, 57170 Savonlinna, Finland
e-mail: Kari.Ullakko@lut.fi

J. Järvinen
Silicom Ltd., Rakovalkeantie 23 D 10, 00670 Helsinki, Finland

1 Introduction

The demands on emerging microfluidic technologies have steadily increased as the field has matured. There is a strong interest in the development of portable devices such as point of care diagnostics (Whitesides 2006), micrototal analysis systems (Manz et al. 1990) and the lab-on-a-chip (Stone et al. 2004). In order to fully realize a portable microfluidic device, its components must be built into the device with minimal dependency on external components. As such, miniaturization and integration of microfluidic technologies is a necessary technological development. An essential element to these devices is the method in which the fluid is moved through the system. In comparison with the other microfluidic components, micropumps are a lagging technology with several devices still being driven by external pumps, such as peristaltic pumps and syringes, which are connected to the device (Laser and Santiago 2004).

One can imagine several qualities that a micropump must have in order for it to be capable of integration within a microfluidic system. It must meet all the expected performance requirements. It should be a simple design with a minimal number of moving mechanical parts and electrical contacts to make manufacturing and integration easier. Furthermore, it must be self-priming so that the micropump can independently and completely control the flow within the microfluidic system. There have been several developments in micropump technologies such as using piezoelectric diaphragms (Smits 1990), acoustic wave (Guttenberg et al. 2005), finger-operated pumps (Qiu et al. 2009; Yang et al. 2010) and several others discussed in Woias's review (2005). Although these micropumps are not suited for integration, recent research has shown new technologies which have more potential.

Kan et al. (2008) has developed a serial-connection multi-chamber piezoelectric micropump that achieves significant flow rates (about 125 μL/s at 400 Hz) and pressures (48.6 kPa) while requiring less voltage (40 V) than traditional piezoelectric micropumps. The disadvantage of this design is that it consists of many mechanical parts and is relatively difficult to manufacture which inhibits its direct integration into a microfluidic system. Sheen et al. (2008) and Wang et al. (2010) present valveless piezoelectric micropumps that have a simple design. Sheen's micropump achieves flow rates of 0.47 μL/s and a pumping pressure of 1.1 kPa, which is insufficient for many microfluidic applications. Wang's micropump has acceptable flow rates (10 μL/s), but also has low pumping pressure (1.4 kPa) and requires a high voltage (150 V). A specific disadvantage of the valveless micropump design is that any pressure differential will cause leaking unless the piezoelectric diaphragm is actively actuated. Additionally, any piezoelectric micropump requires electric contacts to actuate the piezoelectric diaphragm which complicates how they could be integrated into a microfluidic device. Thus, it is clear that further development of micropump technology is needed before it can be reasonably considered as a component that is incorporated into microfluidic devices.

The micropump that is used in this study was first proposed by Ullakko et al. (2012) and is a strong candidate for integration into microfluidic devices. The pump uses primarily a magnetic shape memory (MSM) alloy, Ni–Mn–Ga, as the pumping mechanism, and thus, it is a simple design with minimal parts. It is driven by a magnetic field and does not require direct contact with its power source. It is self-priming and robust, capable of pumping both gas and viscous liquids. These characteristics coupled with its resolution and repeatability make the MSM micropump (MSMM) a strong candidate for an integratable flow control solution within microfluidic systems. In this study, the (MSMM) is further developed, characterized and modeled. Key performance characteristics that are important in microfluidic devices, such as the flow rate, repeatability and maximum pressure, are measured, and the unique qualities of the MSMM are analyzed.

2 Structure and pumping mechanism of the MSM micropump

2.1 Structure of the micropump

Figure 1a is a schematic of the MSMM that was used in this study. The micropump, 17.5 mm × 10 mm × 4.7 mm in size, is composed of three parts: a supporting plate with holes that act as the inlet and outlet, the MSM element which is the body of the pump and an elastomer which seals the working channel of the MSM element. The supporting plate is a 3-mm-thick polycarbonate plate which is the substrate to which the MSM element is anchored. It has two holes (1.5 mm in diameter) that act as the inlet and outlet for the pump. Larger holes (3 mm in diameter) can be seen in Fig. 1a and were used to interface the MSMM with the various experiments. A primer (Dow Corning, 1200 OS) was applied to the surface of the plate which was used to increase the adhesion between the elastomer and the plate. Removable plugs are inserted into the two holes to prevent the elastomer from filling them. The MSM element (10 mm × 2.5 mm × 1 mm) is compressed fully such that it is in a single variant where the shorter crystallographic *c*–axes are all aligned in the long direction of the element. It is then centered and placed over the two holes, and a two-part liquid elastomer (Dow Corning, Sylgard 184) is then poured into the mold, encapsulating the element and covering plate. After the elastomer has cured, the plugs are removed so that the inlet/outlet directly interfaces with the MSM element. The MSMM was then placed between two plates that were clamped together. At this point, the pump is complete and ready to operate.

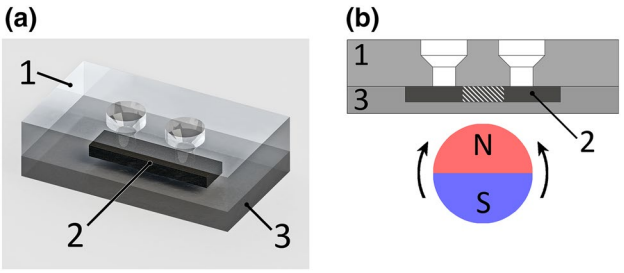

Fig. 1 **a** A 3D rendering of the magnetic shape memory micropump. (MSMM). It consists primarily of three parts: (1) a polycarbonate plate to act as the substrate, (2) the magnetic shape memory material Ni–Mn–Ga which is the working mechanism and (3) the elastomer which seals the channel and prevents leaking. **b** A schematic of the experimental setup. A diametrically magnetized permanent magnet is rotated near the micropump to control the flow of fluid between the inlet and outlet

The elastomer serves multiple purposes in this design. Since it is a liquid when the two parts are combined, it completely encapsulates the MSM element and coats the plate, conforming to any abnormalities and surface defects that are present in either part. Since the plate was previously primed, the elastomer between the MSM element and the plate preferentially adheres to the plate. Therefore, as the shrinkage moves across the element, the MSM material is pulling away from the elastomer which indicates that the liquid is pumped between the elastomer–MSM element interface. In this way, a seal is created that is of

critical importance for the performance of the micropump. The regular magnetic field from the diametrically magnetized cylindrical magnet creates a consistent shrinkage along the MSM element that has the same volume with each cycle. The strength of the magnetic field needed in order to create a shrinkage in the MSM element is dependent upon the twinning stress of the material. For a twinning stress of 0.2 MPa, a magnetic field of 240 mT is needed. For this reason, a diametrically magnetized cylindrical rare earth permanent magnet (NdFeB N52 grade, 6.3 mm OD $\times$ 25.4 mm) with a strong magnetic field, measured to be 500 mT at the magnet's surface, was used to operate the pump.

2.2 The pumping mechanism

A key feature of this micropump is that it is remarkably simple. This is because Ni–Mn–Ga, an MSM alloy, is a material that can replace functions that are normally performed by a system of mechanical parts. In this case, a single piece of Ni–Mn–Ga is the heart of the MSMM, acting simultaneously as the pump, valve and channel. This material changes its shape and dimensions, through a process known as twinning, when a magnetic field of sufficient strength is applied to the material. The magnetic field required for a typical sample with a 0.2 MPa twinning stress is 240 mT, but recent research has shown that the magnetic field could be as low as 30 mT for MSM elements that use a different twinning mechanism (Kellis et al. 2012). The magnetic-field-induced strain can be up to 10 % (Ullakko et al. 1996; Murray et al. 2000; Sozinov et al. 2002) which is two orders of magnitude greater than those of giant magnetostrictive materials, for example Terfenol-D™, and piezoelectric materials. The material can be precisely controlled (Ullakko and Likhachev 2000), actuates rapidly and responds quickly to the applied magnetic field. A unique benefit from drawing energy from a magnetic field is that the MSM element can essentially be controlled by a driving mechanism that is physically separated from the element itself. This greatly simplifies the design and construction of MSM devices by allowing them to be contact-free. With an efficiency of over 90 % (Straka et al. 2011), it is clear why Ni–Mn–Ga has received so much attention as an actuating material.

Typical devices that have utilized Ni–Mn–Ga in the past have applied a uniform magnetic field to the bulk material which causes the entire MSM element to actuate. Only recently has research shown how the material can respond locally, with a predictable twin configuration, when a magnetic field is applied to a small area of the MSM element (Smith et al. 2014a, b). For the micropump presented here, a diametrically magnetized permanent magnet was rotated to create and move an identical magnetic field repeatedly across a section of the MSM element. The element responds accordingly with a specific, reproducible twin configuration which has been called shrinkage. This shrinkage forms at the inlet of the micropump and follows the rotating magnetic field, transporting the volume of liquid to the outlet of the MSMM. The movement of the shrinkage across the MSM element is similar to the mechanism of an animal swallowing. As the magnet rotates, the MSM element immediately in front of the shrinkage contracts, which creates space for the liquid to move forward. Simultaneously, the MSM element immediately behind the shrinkage expands, forcing the liquid forward into the created space. Figure 2 shows experimentally and schematically how the shrinkage moves across the MSM element. Further details about the magnetic field from the permanent magnet, how it creates the shrinkage in the MSM element and how the shrinkage propagates through the MSM element are further discussed by Ullakko et al. (2012).

3 Experimental setup

After the MSMM was constructed, an experimental setup, shown schematically in Fig. 1b, was built for driving the micropump and measuring its performance characteristics. As such, a plastic jig to operate the MSMM was prepared that had a hole, 7 mm in diameter, drilled into it 0.3 mm away from the surface where the MSMM would be placed. The larger hole size provides an air gap between the magnet and jig, therefore minimizing friction. A custom aluminum adapter was machined that connected the permanent magnet to a 6-W brushed DC motor (Maxon Motor AG, A-Max 22) that was used to power the MSMM. It should be noted that one revolution of the magnet is equal to two complete pumping cycles, and that, for the purpose of this paper, the speed at which the pump is operated will be referred to as pumping cycles per second, or pumping frequency. The speed that the motor was rotating was measured by an optical encoder (Honeywell, Optoschmitt sensor) and an oscilloscope (Metrix, Scopix III OX 7204). The motor, optical encoder and jig were fastened to a rigid plate that was held in place. The highest pumping frequency that was used in these experiments was 270 Hz due to limitations of the experimental setup. The MSM material itself has been shown to actuate and respond to an applied magnetic field very rapidly, which implies that higher frequencies could be used (Smith et al. 2014a, b).

In order to measure the volume of liquid that was pumped, small pipettes were attached to the inlet and outlet holes of the MSMM to act as a reservoir for the liquid as it was being pumped during the experiments. Two liquids were used for the flow rate measurements: pure water and a 60 %wt. glycerol solution. This glycerol solution, at

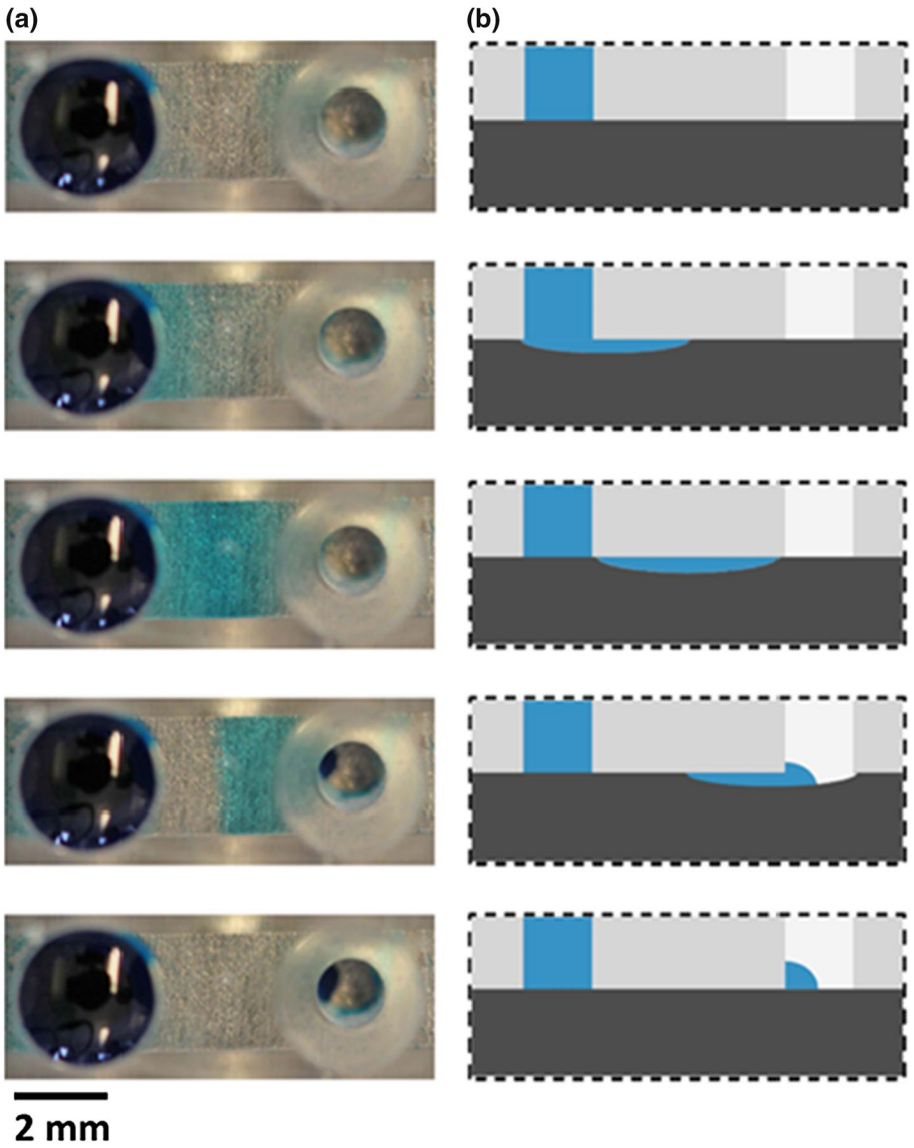

Fig. 2 **a** From *top to bottom*, *top-view* photos of a single cycle of the micropump. The shrinkage can be distinctly seen moving from the inlet (*left*) to the outlet (*right*). **b** A correlating schematic showing the side view of the micropump as the shrinkage moves from the inlet to the outlet

room temperature, is about ten times more viscous than water (Segur and Oberstar 1951) and was used to experimentally model the pumping of more viscous fluids such as blood, plasma or serum. A volume of 0.5 ml of liquid was pumped at a known frequency and the time recorded in order to measure the flow rate of the pump. The liquid was then pumped back into the inlet pipette by reversing the rotation of the magnet so that the experiment could be repeated. By doing so, the same liquid was pumped for each measurement rather than replacing the original liquid with a new volume. The flow rate was then calculated as flow rate = volume/time. From the same data, the volume per cycle, V_c, could also be calculated for each of the frequencies by the equation V_c = volume/(time × frequency). The repeatability of the micropump was measured in a similar fashion. The time to pump the same volume of water at a frequency of 100 Hz was measured multiple times to determine the performance repeatability of the pump.

A customized closed fluid system, in which the pressure could be continuously regulated, was connected to a similarly constructed MSMM in order to measure the pressure that the pump could operate against. The pump was operated at 100 Hz in the same manner as the flow rate experiments. The pressure within the system was incrementally increased from atmospheric pressure until the pump could no longer move the fluid against the pressure. Since the MSMM could also be used as a valve, it was of interest to see how much pressure it could hold when it was not in active operation. As such, the motor was turned off so that the MSM material was in a closed position and the pressure further increased until backflow through the inlet was observed.

An important parameter of a micropump is how much power is required to operate it. As such, two tests were conducted at room temperature to determine the electric power required to operate the MSMM: the power consumed without the load of the MSMM and then the power consumed when the MSMM was being operated. To determine the former, the current–voltage characteristics of the motor were measured when the rotor was locked to obtain the terminal resistance, R, of the motor. The voltage and current of the motor were then measured at various motor speeds without the MSMM in place to determine the power consumed by the motor, P_{NoLoad}. Finally, a similar experiment was conducted with the MSMM in place to determine the additional power consumed by the motor with the MSMM in place, P_{Load}. From these data, the power consumption of the MSMM itself, P, could be calculated:

$$P = \Delta P_{\mathrm{m}} - \Delta P_{\mathrm{J}} \tag{1}$$

where ΔP_{m}, the difference between the power consumed by the motor with and without the load of the MSMM, and ΔP_{J}, the difference between the joule heat dissipated by the motor with and without the load of the MSMM, are calculated as

$$\Delta P_{\mathrm{m}} = V_{\mathrm{Load}} I_{\mathrm{Load}} - V_{\mathrm{NoLoad}} I_{\mathrm{NoLoad}} \tag{2}$$

$$\Delta P_{\mathrm{J}} = R\left(I_{\mathrm{Load}}^2 - I_{\mathrm{NoLoad}}^2\right) \tag{3}$$

Since some fluids that are used in microfluidics are temperature-sensitive, the increase in temperature during the operation of the MSMM was measured using two methods. For each of these experiments, the temperature was measured over a period of 10 mins using an infrared sensor (Fluke, VT04 Visual IR thermometer) while the MSM element was being actuated at 100 Hz. No liquid was pumped during these temperature measurements since it would act as a coolant. In the first test, the temperature increase in the MSMM used in the previous tests was measured. However, concerns were raised that the infrared sensor was measuring the surface temperature of the polycarbonate plate which could be different than the temperature of the element itself. A second test was conducted on a different MSM element that was similar to the first except that it was not encased in an elastomer or polycarbonate plate. This allowed for a direct infrared measurement of the surface of the MSM element. This was deemed important because it is the surface of the MSM element that would be contacting the fluid that was being pumped and not the outer surface of the polycarbonate plate.

Optimization of the MSMM is of interest in the future and as such, a model was created, with the same dimensions as the MSMM, which simulated the flow of the liquid caused by the closing of the shrinkage at the outlet. The fluid dynamics would be the same on both halves of the outlet and shrinkage if the full geometry was used, being mirrored along the axis of symmetry. For this reason, only half of the shrinkage and outlet were modeled which simplified the model and reduced the computational expenditure. The finite element analysis software Elmer (developed by the IT Center for Science, Finland) was used to create a 2D computational fluid dynamics model of water being pumped through the outlet by a parabolic shrinkage that was moving in the same direction as the axis of the outlet, which was modeled to be 1.5 mm in diameter. This reasonably correlates to what occurs between frames 4 and 5 of Fig. 2b assuming the outlet is completely filled with fluid. A mesh of 26,000 elements was used in this model which was updated at each time step of 2.0×10^{-4} s. The fluid being moved was assumed to be incompressible and was modeled by the transient Navier–Stokes equations which were linearized using Newton's method. The linearized system was solved iteratively using BiCGStab and ILU preconditioning. Time was discretized by the second-order BDF and space discretized by the stability of the rendered finite elements.

4 Results and discussion

4.1 Pumping performance

The flow rate was first measured at a pumping frequency of 30 Hz and then at subsequent frequency intervals of 30 up to 270 Hz for the water measurements and up to 240 Hz for the 60 %wt. glycerol solution. Figure 3 is a graph that shows the flow rate as a function of the

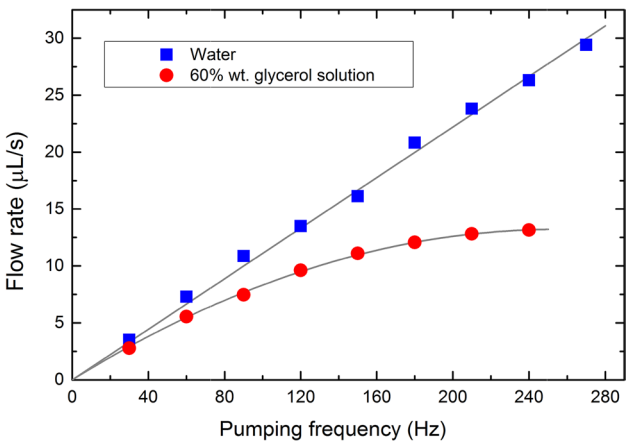

Fig. 3 A graph of the flow rate of the micropump as a function of its pumping frequency. The flow rate of the water solution (*blue squares*) follows a linear trend with a slope of 111 nL/cycle. The flow rate of the glycerol solution approaches an asymptotic value of about 13.2 μL/s at 240 Hz

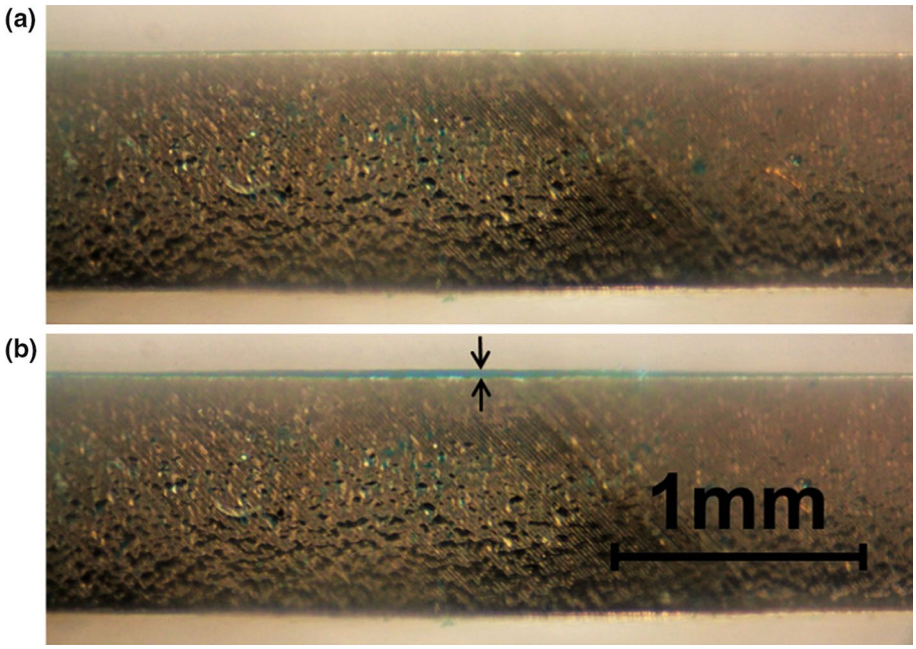

Fig. 4 **a** An optical micrograph of the *side view* of the micropump when there is no shrinkage present and the element is in a closed orientation. **b** An optical micrograph of the *side view* of the micropump when a shrinkage is formed and the element is in an opened orientation. The *two arrows* in the middle of the photo emphasize the shrinkage, filled with a *blue liquid*, which has a depth of approximately 30 μm

pumping frequency for both liquids. In the figure, the flow rate for water (blue squares) is quasi-linear. The volume pumped per cycle, which is the slope of the fitted line, can be calculated by dividing the flow rate by the pumping frequency. Including experimental error, the volume of water pumped per cycle is calculated to be 110 nL ± 15 nL per pumping cycle which correlates to the resolution of the MSMM. The flow rate curve for the glycerol solution (red circles) approaches an asymptotic value of about 13.2 μL/s at 240 Hz. It was originally hypothesized that the volume pumped per cycle would be the same for liquids. However, in the case of glycerol, the volume pumped per cycle decreases as the pumping frequency increases. This is due to surface effects and viscosity which become a limiting factor that inhibits the flow of the liquid through the MSMM. It is expected that the flow rate curve for water would also follow a similar trend as the glycerol solution curve at significantly higher frequencies. Figure 4 is an optical micrograph of the side view of the shrinkage in both its closed (Fig. 4a) and opened (Fig. 4b) position. The depth of the shrinkage is approximately 30 μm which explains why the surface effects become dominant in the glycerol solution. The volume of the shrinkage, calculated from the micrographs of the shrinkage profile, is 130 nL. This calculated volume of the shrinkage correlates well with the experimental volume that was determined from the flow rate measurements of water. The time necessary to pump 0.5 mL of water at 100 Hz was 40.3 s with a mean square error of ± 2 %. Given that a portion of this error is due to the methods of measurement, it is clear that the MSMM has high performance repeatability. This repeatability measurement also reinforces the conclusion that the volume of the shrinkage is the same with each cycle.

The current and voltage of the motor, once without the MSMM and once with the MSMM being operated, were measured at a pumping frequency of 20 Hz and then at subsequent frequency intervals of 20 up to 180 Hz. Using Eqs. 1 through 3, the increase in the motor's power consumption was calculated for each measured frequency. It was found that the additional power consumed due to the MSMM is linearly proportional to the pumping frequency, with 0.77 mJ of energy being used per cycle. This corresponds to a power consumption of 208 mW at 270 Hz. Within experimental error, there were no differences in the additional power consumed due to the MSMM based on the fluid (air, water and 60 %wt. glycerol solution) that was being pumped. This indicates that the power is being used almost entirely to actuate the MSM element and that the resistance of the fluid is negligible in comparison. Furthermore, this reinforces the previous conclusion that the shrinkage volume is the same regardless of the fluid or the pumping frequency.

A temperature increase of 3° ± 0.5 °C was observed on the surface of the MSMM after running it, without liquid, for 10 min at 100 Hz. In order to ensure that this temperature measurement was accurate, a second, similar experiment was conducted on a similar MSM element that was not encapsulated by elastomer or a plate. The surface temperature of the MSM element increased 2.5 °C after being actuated for 10 min at 100 Hz. The similarity of this second experiment validates the first experiment on the MSMM. It should be noted that any liquid that is being pumped through the MSMM would act as a coolant

for the MSM element. The actual temperature increase in the liquid would therefore be significantly lower than what was observed in these experiments. This indicates that the MSMM would be able to pump temperature-sensitive fluids, such as biological samples, without adverse effects.

Fatigue characteristics of the micropump are also important to characterize. The same MSMM was used in all of the experiments reported in this paper. The performance of the pump in the final experiments was similar to its performance in the first experiments, and it is estimated that the pump was actuated on the order of millions of cycles. It was observed, through optical microscopy, that there were no cracks or other visible signs of fatigue on the surface of the MSM element used in the pump. These fatigue data correlate well with previous research on the fatigue properties of Ni–Mn–Ga, which demonstrates that an MSM element can actuate up to 2×10^9 cycles (Aaltio et al. 2010).

The MSMM continued to pump with a pressure difference of 150 kPa between the inlet and outlet. However, the MSMM can also act as a valve, in which case it can maintain up to 200 kPa of pressure. A decrease in the flow rate of the MSMM was qualitatively observed that correlated to the increase in pressure. It should be noted that the theoretical limit that the MSMM should be able to pump against is 2 MPa since this is the blocking stress of the MSM material (Murray et al. 2001). The current limitation regarding the pump's operating pressure is therefore the sealing. It is expected that improvement in the sealing technology will further prevent backflow and therefore increase the pressure that the MSMM can operate against and maintain.

4.2 Simulation of the outlet flow

Figure 5a schematically shows the geometry that was used in the computational fluid dynamics model. The shrinkage was modeled to be parabolic to resemble the shape that was experimentally observed, which can be seen in Fig. 4. The geometry was particularly challenging due to the dimensions of the shrinkage in comparison with the outlet. The depth of the shrinkage is significantly smaller than the outlet's dimensions, whereas the length of the shrinkage is larger. Additionally, the fluid flow was created by a moving boundary rather than inlet/outlet conditions. The moving boundary created further difficulties because the mesh that was initially rendered quickly became distorted at the interface between the outlet and shrinkage. To solve this, an artificial boundary was placed along the interface between the outlet and shrinkage and different conditions set for each area. Within the shrinkage, the dimensions of individual mesh elements changed with time whereas the mesh elements in the outlet were static. This prevented severe mesh distortion and allowed the model to successfully be solved.

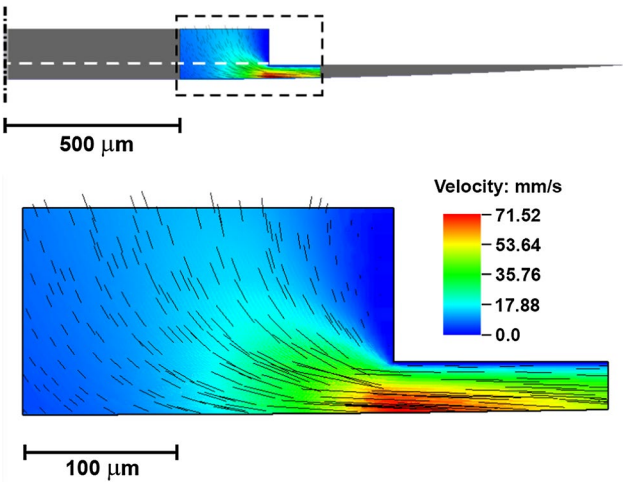

Fig. 5 **a** The geometry that was used in the computational fluid dynamics. To simplify the simulation, only half of the shrinkage was modeled. The *black, vertical dash-dot line* indicates the axis of mirrored symmetry. The area of interest is outlined by the *black dashed rectangle*. The *white dashed line* is the boundary between the outlet and shrinkage mesh elements. **b** The results of the simulation within the area of interest. The maximum velocity shown is 71.52 mm/s which is located at the bottom of the shrinkage beneath the corner of the outlet. The *black lines* indicate the direction and magnitude of the flow, which is from *right to left*

Due to the geometry, it was difficult to clearly see the results of the simulation when viewing the entire model. As such, an area of interest was chosen (the boxed area in Fig. 5a) which is centered on the corner between the shrinkage and outlet areas. This area was chosen because this is where the velocity magnitude is the highest and where the velocity direction changes the most. Figure 5b shows the velocity field obtained from the simulation at a single time step. As expected, the maximum velocity occurs along the shrinkage boundary directly beneath the corner of the shrinkage and outlet areas. It was observed that the magnitude of the velocity vectors changed with time but not their direction. The velocity magnitude increased with time as the shrinkage volume decreased with a maximum speed of 71.5 mm/s when calculated for a pumping frequency of 100 Hz. The black lines in the figure are the velocity vectors which indicate the direction of the flow, which is from the right to the left moving toward the outlet.

The difference between the shrinkage volume and flow rates between the simulation and the experimental results is 25 %. These errors are reasonable given the assumptions and simplifications made in the model. Therefore, the simulation results reasonably model the experiment and assists in understanding the fluid dynamics that are occurring within the MSMM. This model is the first step toward optimizing the design of the MSMM. For example, the outlet geometry can be optimized, such as by

decreasing the outlet diameter or changing its interface, while minimizing the pressure within the micropump. The effects of other shrinkage geometries can be modeled and understood prior to investing in changing the MSMM. Fluid properties such as compressibility and viscosity can be manipulated to determine the limitations of the MSMM. The model could be further developed to analyze the entire MSMM, its pumping mechanism and potentially the microfluidic system to which it would be integrated.

4.3 Pump characteristics

It is important to emphasize that the MSMM has several qualities that make it a competitive technology beyond the quantifiable specifications mentioned previously. One such characteristic is its multi-functionality. The MSMM acts simultaneously as both a valve and a pump. This is because the MSMM is designed so that the MSM material is normally in the wider variant which closes the working channel. The MSM material will only contract into its thinner variant when a perpendicular magnetic field directly affects it and creates a shrinkage. Furthermore, the shrinkage length is shorter than the distance between the inlet and outlet so that there is never a completely open channel between the inlet and outlet. This means that the liquid cannot be transferred between the inlet and outlet without being actively transported by the shrinkage. The significance of this characteristic is further realized considering the MSMM can pump in both directions. The direction that the MSMM pumps can be reversed simply the direction of the magnetic field source. The MSM material seals the working channel of the pump regardless of its direction of operation. In this way, the MSM material replaces mechanical valves and is superior to one-way check valves that are commonly used in microfluidic devices.

The trend in microfluidic systems is to create the most value in the smallest amount of space, and, as such, simplicity is an essential quality for microfluidic devices. The multi-functionality of the MSMM increases its value in a microfluidic system. The value of the MSMM is further increased due to both its small size and the simplicity of its design; it is fundamentally a piece of MSM material that is placed within a microfluidic channel. Furthermore, the MSMM does not require electrical contacts and is powered externally by a magnetic field. These qualities mean the MSMM is a microfluidic device that lends itself to simple integration into microfluidic systems. The pump could even be integrated into existing designs that need additional flow control with minimal reengineering of the microfluidic system.

Precision and accuracy are important characteristics to a micropump. The pumping precision of the MSMM is dependent upon discrete volumes, each the same as the other, that are transferred between the inlet and outlet. This means that the micropump has a discrete resolution based upon the volume that is transported by the shrinkage. Since the size of the shrinkage generated in the MSMM is dependent upon both the magnetic field *and* the size of the MSM element, the pumping resolution can be further improved should an application require increased accuracy or smaller volumes pumped per cycle. To demonstrate this concept, an experiment was conducted that demonstrated that Ni–Mn–Ga retains the MSM effect even when it is 6 μm thick. This clearly shows that MSM technology is scalable. The size of the permanent magnet can also be scaled with the MSMM as long as its magnetic field is still sufficiently strong. However, since the MSMM is physically independent from the permanent magnet and motor, it can still be scaled down and integrated into microfluidic devices while still using the same permanent magnet and motor.

The MSMM is a very robust design because it not only pumps liquids that are substantially more viscous than water, such as the 60 %wt. glycerol solution, but it can also pump air. While conducting the flow rate experiments, the pump transitioned smoothly to pumping air after the liquid volume at the inlet was depleted. This is significant because it demonstrates that the MSMM will continue to operate well even if the liquid is not homogeneous or has bubbles present in the mixture. Furthermore, the same technology can be used in applications that need flow control of gas within the system.

Table 1 Summary of the quantitative and qualitative characteristics of the MSM micropump

Summary of the measured MSM micropump characteristics		
Quantitative		Qualitative
Maximum pressure	150 kPa	Multifunctional—valve & pump
Flow rate	0–30 μL/s at 0–270 Hz	Simple design
Volume per cycle (Resolution)	110 nL	Scalable
Repeatability	2 %	Contact-free
Power consumption per cycle	0.77 mJ/cycle (208 mW at 270 Hz)	Discrete volume resolution
Fatigue	Millions of cycles	Pumps gas and viscous liquids

Details of each can be found in Sects. 4.1 and 4.3, respectively

5 Conclusions

Using the MSM alloy Ni–Mn–Ga, a micropump was developed and characterized. Table 1 summarizes the quantitative and qualitative characteristics of the micropump. There are several advantages that make the MSMM unique and a promising technology. Its quantitative performance meets the expectations of microfluidic devices and competitive technologies. It has additional value compared to other micropump technology because its flow rate can be reversed *and* it simultaneously operates as both a valve and pump. It has a variable flow rate according to the cycling frequency which is controlled externally via a magnetic field. This means the MSMM is simple, contact-free and requires no electrical contacts to the micropump itself. The technology has been proven to be scalable which indicates that its size can be reduced to the dimensions of a microfluidic channel. Furthermore, it has been shown that the pump is self-priming and robust, capable of pumping gas and even viscous liquids. These attributes, combined with its simple design, indicate that the MSM micropump will be capable of integrating directly into the microfluidic channel itself. These characteristics make the MSMM well suited for applications such as lab-on-a-chip and point of care diagnostic microfluidic systems. It is expected that the MSMM will both enable the development of new technologies as well as provide greater freedom for microfluidic system designers.

References

Aaltio I, Soroka A, Ge Y, Söderberg O, Hannula S-P (2010) High-cycle fatigue of 10 M Ni–Mn–Ga magnetic shape memory alloy in reversed mechanical loading. Smart Mater Struct 19:075014. doi:10.1088/1726/19/7/075014

Guttenberg Z et al (2005) Planar chip device for PCR and hybridization with surface acoustic wave pump. Lab Chip 5:308–317. doi:10.1039/B412712A

Kan J, Tang K, Liu G, Zhu G, Shao C (2008) Development of serial-connection piezoelectric pumps. Sens Actuators A Phys 144:321–327. doi:10.1016/j.sna.2008.01.016

Kellis D, Smith A, Ullakko K, Müllner P (2012) Oriented single crystals of Ni–Mn–Ga with very low switching field. J Cryst Growth 358:64–68. doi:10.1016/j.jcrysgro.2012.08.014

Laser DJ, Santiago JG (2004) A review of micropumps. J Micromech Microeng 14:R35. doi:10.1088/0960-1317/14/6/R01

Manz A, Graber N, Widmer HM (1990) Miniaturized total chemical analysis systems: a novel concept for chemical sensing. Sens Actuators B Chem 1:244–248. doi:10.1016/0925-4005(90)80209-i

Murray SJ, Marioni MA, Allen SM, O'Handley SC, Lograsso TA (2000) 6 % magnetic-field-induced strain by twin-boundary motion in ferromagnetic Ni–Mn–Ga. Appl Phys Lett 77:886–888. doi:10.1063/1.1306635

Murray SJ, Marioni M, Tello PG, Allen SM, O'Handley RC (2001) Giant magnetic-field-induced strain in Ni–Mn–Ga crystals: experimental results and modelling. J Magn Magn Mater 226:945–947. doi:10.1016/S0304-8853(00)00611-9

Qiu X et al (2009) Finger-actuated, self-contained immunoassay cassettes. Biomed Microdevices 11:1175–1186. doi:10.1007/s10544-009-9334-4

Segur JB, Oberstar HE (1951) Viscosity of glycerol and its aqueous solutions. Ind Eng Chem 43:2117. doi:10.1021/ie50501a040

Sheen HJ, Hsu CJ, Wu TH, Chang CC, Chu HC, Yang CY, Lei U (2008) Unsteady flow behaviors in an obstacle-type valveless micropump by micro-PIV. Microfluid Nanofluidics 4:331–342. doi:10.1007/s10404-007-0189-9

Smith AR, Tellinen J, Müllner P, Ullakko K (2014a) Controlling twin variant configuration in a constrained Ni–Mn–Ga sample using local magnetic fields. Scr Mater 77:68–70. doi:10.1016/j.scriptamat.2014.01.028

Smith AR, Tellinen J, Ullakko K (2014b) Rapid actuation and resposne of Ni–Mn–Ga to magnetic-field-induced stress. Acta Mater 80:373–379. doi:10.1016/j.actamat.2014.06.054

Smits JG (1990) Piezoelectric micropump with three valves working peristaltically. Sens Actuators A Phys 21:203–206. doi:10.1016/0924-4247(90)85039-7

Sozinov A, Likhachev AA, Lanska N, Ullakko K (2002) Giant magnetic-field-induced strain in NiMnGa seven-layered martensitic phase. Appl Phys Lett 80:1746–1748. doi:10.1063/1.1458075

Stone HA, Stroock AD, Ajdari A (2004) Engineering flows in small devices: microfluidics toward a lab-on-a-chip. Annu Rev Fluid Mech 36:381–411. doi:10.1146/annurev.fluid.35.050802.122124

Straka L, Hänninen H, Soroka A, Sozinov A (2011) Ni–Mn–Ga single crystals with very low twinning stress. J Phys Conf Ser 303:012079. doi:10.1088/1742-6596/303/1/012079

Ullakko K, Likhachev AA (2000) Magnetic-field-controlled twin boundaries motion and giant magneto-mechanical effects in Ni–Mn–Ga shape memory alloy. Phys Lett A 275:142–151. doi:10.1016/S0375-9601(00)00561-2

Ullakko K, Huang JK, Kantner C, O'Handley RC, Kokorin VV (1996) Large magnetic-field-induced strains in Ni2MnGa single crystals. Appl Phys Lett 69:1966–1968. doi: 10.1063/1.117637

Ullakko K, Wendell L, Smith A, Müllner P, Hampikian G (2012) A magnetic shape memory micropump: contact-free, and compatible with PCR and human DNA profiling. Smart Mater Struct 21:115020. doi:10.1088/0964-1726/21/11/115020

Wang SS, Huang XY, Yang C (2010) Valveless micropump with acoustically featured pumping chamber. Microfluid Nanofluidics 8:549–555. doi:10.1007/s10404-009-0533-3

Whitesides GM (2006) The origins and the future of microfluidics. Nature 442:368–373. doi:10.1038/nature05058

Woias P (2005) Micropumps—past, progress and future prospects. Sens Actuators B Chem 105(1):28–38. doi:10.1016/j.snb.2004.02.033

Yang W et al (2010) Fabrication of a hydrophilic poly (dimethylsiloxane) microporous structure an its application to portable microfluidic pump. Jpn J Appl Phys 49:06GM01. doi:10.1143/JJAP.49.06GM01